Magnetic Stimulation Coil and Circuit Design

Kent Davey*, *Senior Member, IEEE,* and Charles M. Epstein

***Abstract*—A detailed analysis of the membrane voltage rise commensurate with the electrical charging circuit of a typical magnetic stimulator is presented. The analysis shows how the membrane voltage is linked to the energy, reluctance, and resonant frequency of the electrical charging circuit. There is an optimum resonant frequency for any nerve membrane depending on its capacitive time constant. The analysis also shows why a larger membrane voltage will be registered on the second phase of a biphasic pulse excitation [1]. Typical constraints on three key quantities voltage, current, and silicone controlled rectifier (SCR) switching time dictate key components such as capacitance, inductance, and choice of turns.**

***Index Terms*—Action potential, electric field, magnetic stimulation, nerve.**

I. Introduction

In 1991, Barker *et al.*, wrote an excellent study on the effect of current waveform rise time in determining neural excitation [2]. Following the suggestion of Plonsey [3], they modeled the nerve membrane as a parallel capacitance and resistance, with an intracellular and extracellular resistance providing the closure path for any induced or injected currents. The energy necessary to achieve threshold stimulation was measured as a function of B field rise time. Threshold stimulation energy continued to drop with reduced rise time, i.e., increased resonance frequency of the magnetic stimulator. Their methods were useful in predicting nerve membrane time constants.

Magnetic stimulation requires moving enough charge through an electrically sensitive nerve membrane to depolarize it [4]; this means that the membrane voltage must be increased from its normal resting negative potential. Many authors have attempted to offer guidelines for producing energy efficient stimulation coils [5]–[7], as well in the modeling of these coils [8]. Roth and Basser were among the first to actually model the stimulation of a single fiber by electromagnetic induction [9].

The object of this research is to offer design considerations from coupling analytically the electromagnetic circuit to that within the nerve. Among the results will be suggestions about the value of using biphasic excitation, and the importance of choosing the desired resonant frequency of the circuit. Actual core/coil design considerations are outside the scope of this paper. The analysis will focus on ferromagnetic core coils, but the approach and conclusions are applicable to air core coils as well.

Manuscript received October 7, 1999; revised June 23, 2000. This work was supported by Neotonus, Inc., Marietta, GA 30067 USA. *Asterisk indicates corresponding author*.

*K. Davey is with Neotonus, Inc., 2275 Turnbull Bay Rd., New Smyrna Beach, FL 32168-5941 USA (e-mail: kdavey@neotonus.com).

C. M. Epstein is with the Department of Neurology, Emory University School of Medicine, Atlanta, GA 30322 USA.

Publisher Item Identifier S 0018-9294(00)08816-9.

II. Circuit Considerations

The power electronics of electromagnetic stimulator devices revolves around a capacitor driving current into the inductance of the stimulator core. The stimulator circuit is depicted in Fig. 1 with Fig. 1(a) being the full circuit, and Fig. 1(b) being a simplified equivalent. A dc charged capacitor C is allowed to resonate a complete cycle with the inductance comprising the core head. Were there no winding resistance, this would mean that the capacitive energy 1/2 CV^2 would shift to inductive energy 1/2 LI^2, and then reverse back into the capacitor; the full wavelength would require a time $\tau = 2\pi\sqrt{LC}$.

The magnetic flux from the inductor core is driven into biological tissue; the time changing flux will induce a voltage through the tissue linked by the flux. Of course only a fraction of that flux will link a circuit comprised of the intracellular and extracellular space around a nerve through the membrane wall. This biological circuit is depicted in Fig. 2. The induced voltage is only a fraction of the flux linking the iron core winding. The membrane is characterized by a low permeability/mobility to ion flow in its resting state. Note that the model focuses on a subthreshold state over a long nerve length. The capacitance of the membrane wall can be expressed in terms of its permittivity ε for a per unit axial length ℓ, having radius r, and thickness Δ as

$$C_m = \frac{\varepsilon 2\pi r\ell}{\Delta}. \tag{1}$$

The membrane resistance R_m can be expressed in terms of the membrane wall thickness Δ and the membrane wall conductivity σ_m as

$$R_m = \frac{\Delta}{\sigma_m 2\pi r\ell}. \tag{2}$$

The intracellular resistance per unit length ℓ can be written in terms of the intracellular conductivity σ_i

$$R_i = \frac{\ell}{\sigma_i \pi r^2}. \tag{3}$$

The extracellular resistance R_e is very small since the volume of the extracellular space is large.

III. Analysis

The problem degenerates to solving both a magnetic circuit and a coupled biological circuit. Because the current in the biological tissue is so very small, the problem is not truly a coupled circuit problem since the biological circuit current does not affect the magnetic circuit. Henceforth, lower case i will be used for current $I(t)$ in the time domain, while upper case I will be

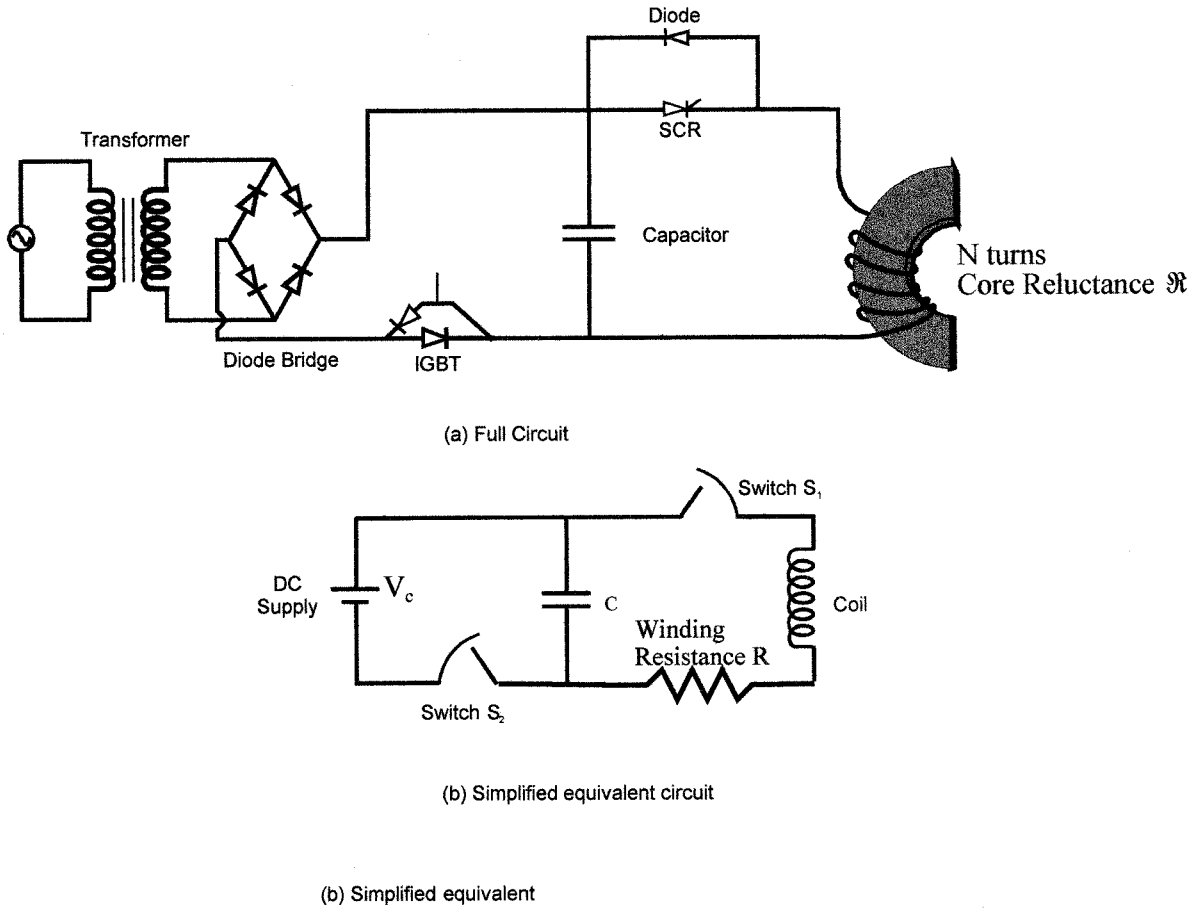

Fig. 1. Circuit for an iron core magnetic stimulator.

used for current $I(s)$ in the Laplace domain. The current i in the magnetic circuit satisfies the differential equation

$$\begin{aligned} L\frac{di^2}{dt^2} + R\frac{di}{dt} + \frac{i}{C} &= 0 \\ \frac{di}{dt}(t=0) = \frac{V_C}{L}, \quad i(t=0) &= 0. \end{aligned} \tag{4}$$

Taking the Laplace transform and using $I(s)$ for the transformed current yields the following

$$I(s) = \frac{V_C}{Ls^2 + Rs + \dfrac{1}{C}}. \tag{5}$$

The flux linking the magnetic core winding is a function of the reluctance $\Re$ of the magnetic circuit and the turns N as

$$\Phi = \frac{Ni}{\Re}. \tag{6}$$

The induced voltage in the biological circuit will be related to a small fraction δ of the total flux through its time rate of change; in Laplace domain space, this becomes

$$V_{ind} = \frac{d}{dt}\left(\frac{\delta Ni}{\Re}\right) = \frac{s\delta NI(s)}{\Re}. \tag{7}$$

Thus, the induced voltage becomes

$$V_{ind}(s) = \frac{s\delta NV_C/\Re}{Ls^2 + Rs + \dfrac{1}{C}}. \tag{8}$$

Of particular interest is the nerve membrane voltage V_m. Kirchoff's voltage law written for the biological circuit is

$$\frac{V_m - V_{ind}}{R_i + R_e} + \frac{V_m C_m s}{2} + \frac{V_m}{2R_m} = 0. \tag{9}$$

Rearranging terms yields the result

$$V_m = \frac{\dfrac{\delta s N V_C}{\Re}\left(\dfrac{2R_m}{2R_m + R_i + R_e}\right)}{\left(Ls^2 + Rs + \dfrac{1}{C}\right)(1 + s\tau_m)} \tag{10}$$

where

$$\tau_m \frac{C_m R_m (R_i + R_e)}{2R_m + R_i + R_e} \approx C_m R_m = \frac{\varepsilon}{\sigma_m}.$$

Here the limit has been taken for large ℓ, where τ_m is dependent only on the constitutive properties of the membrane.

Before processing (10) fully, the reader should note that the emphasis in this paper is not propagation, but subthreshold conditions as discussed in [3]. The membrane voltage cannot be changed instantly; charge must accumulate on either side of the membrane wall, a fact well represented by the RC capacitor

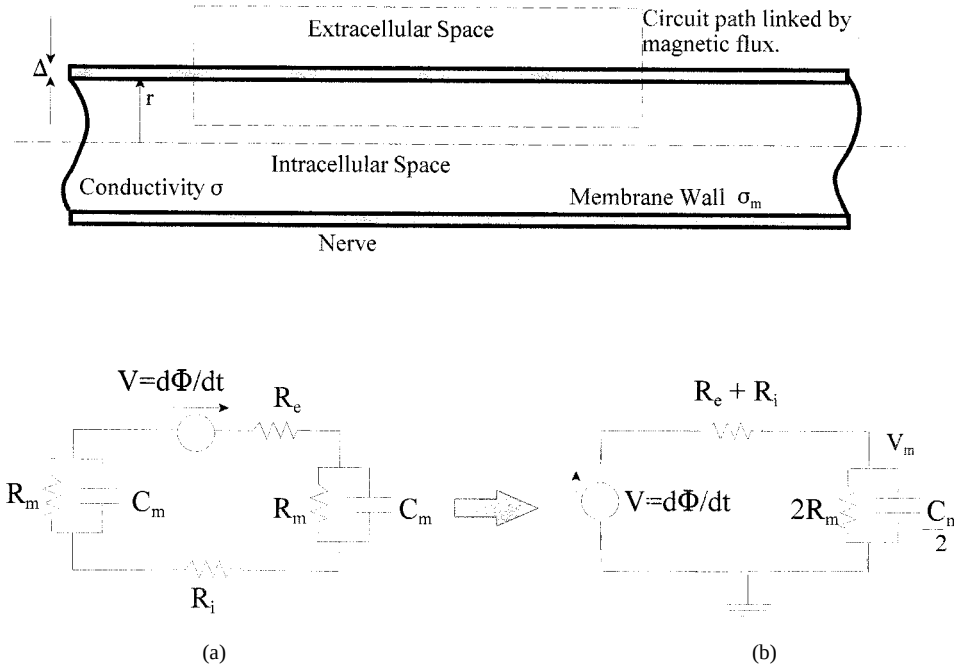

Fig. 2. Biological tissue demonstrating how a changing magnetic flux induces a voltage within a nerve fiber. (a) Electrical representation of a two-patch subblock of the membrane wall. (b) Equivalent electrical circuit.

model. The equivalent neural time constant of that circuit was the primary emphasis in [2]. It is the dynamics of the charging of the membrane to initiate the action potential that is of primary interest. Additional subblocks could be employed in Fig. 2(a) to more finely represent the nerve. But this would only serve to alter the parameter δ, and highlight the fact that the equivalent intracellular multiblock resistance is much greater than the trans-cellular membrane resistance.

The energy W delivered to the magnetic circuit is

$$W = \tfrac{1}{2} C V_C^2 \tag{11}$$

and the resonant resistance free frequency is

$$\omega = \frac{1}{\sqrt{LC}}. \tag{12}$$

In terms of these variables the numerator multiplier of (10) can be rewritten in terms of energy as

$$s\delta N V_C/\Re = s\delta\sqrt{\frac{L}{\Re}}\, V_C = s\delta\frac{\sqrt{LC}\,\sqrt{C}V_C}{C\sqrt{\Re}} = s\delta\frac{\sqrt{2W}\,\omega L}{\sqrt{\Re}}. \tag{13}$$

Here use has been made of the fact that $L = N^2/\Re$. For very short nerve fibers, R_m is a dominant resistance, but for very long fibers with large ℓ, the limit examined in (10)

$$\frac{2R_m}{2R_m + R_i + R_e} \approx \frac{2R_m}{R_i}. \tag{14}$$

For what follows, the resistance ratio $(2R_m)/R_i$ will be absorbed into the factor δ. Finally, the membrane voltage can be written in terms of the maximum circuit energy W and the resonant frequency ω as

$$V_m(s) = \frac{s\delta\sqrt{2W}\omega/\sqrt{\Re}}{\left(s^2 + \dfrac{s}{\tau_L} + \omega^2\right)(1 + s\tau_m)} \tag{15}$$

where the term τ_L has been introduced to represent the L/R time constant. The inverse Laplace transform delivers the membrane voltage as a function of time as is shown in (16) at the bottom of the page, where $\beta \equiv \frac{1}{2}\left((4\omega^2\tau_L^2 - 1)/(\tau_L^2 t)\right)^{1/2}$. Since (16) is quite detailed, it is best to examine V_m for a fixed energy W, magnetic reluctance $\Re$, and flux fraction δ. Typical values for the circuit are $R = 12.6$ mΩ, L =20 μH, and for the membrane, $\tau_m = 100$ μs. The membrane voltage for these parameters is shown in Fig. 3 with $\delta(W/\Re)^{1/2} = 1$. Note that the absolute value of the second negative peak is greater than the first positive peak. Also note that the middle resonant frequency

$$V_m(t) = \delta\sqrt{\frac{2W}{\Re}}\,\omega\,\frac{(4\omega^2\tau_L^2 - 1)\left(e^{-(t/2\tau_L)}\cos(\beta) + \dfrac{e^{-(t/2\tau_L)}(2\tau_L\tau_m\omega^2 - 1)\sin(\beta)}{\sqrt{4\omega^2\tau_L^2 - 1}} - e^{-(t/\tau_m)}\right)}{4\omega^4\tau_m^2\tau_L^2 + \omega^2(4\tau_L^2 - 4\tau_L\tau_m - \tau_m^2) + \left(\dfrac{\tau_m}{\tau_L} - 1\right)} \tag{16}$$

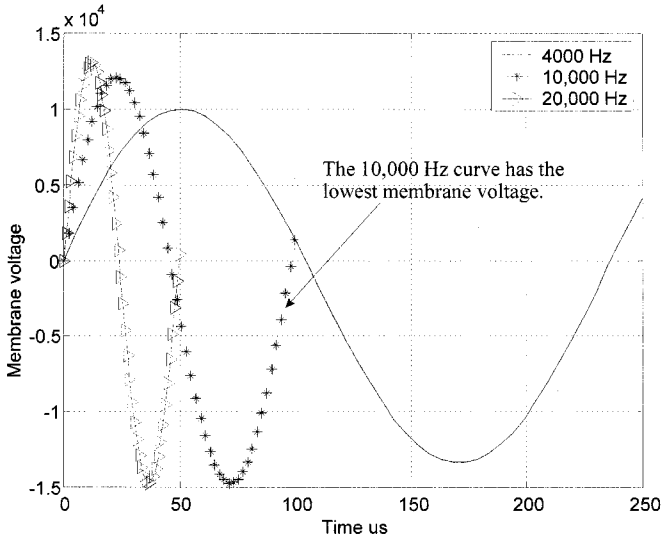

Fig. 3. Membrane voltage for three resonant frequencies.

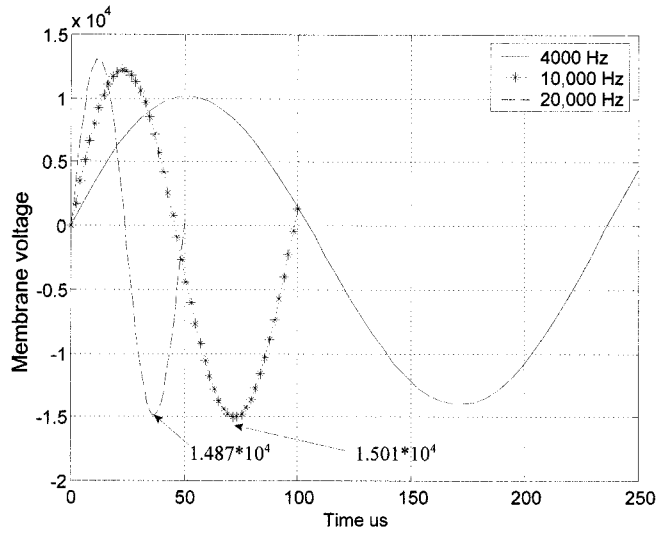

Fig. 4. Membrane voltage with no magnetic circuit winding resistance for three resonant frequencies.

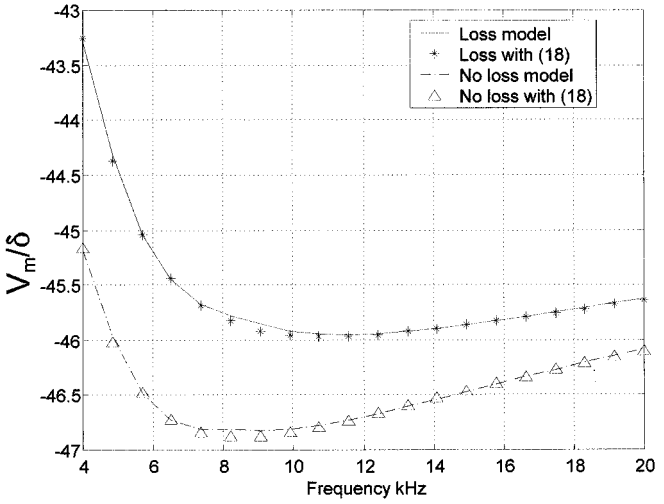

Fig. 5. Minimum membrane voltage as a function of resonant frequency.

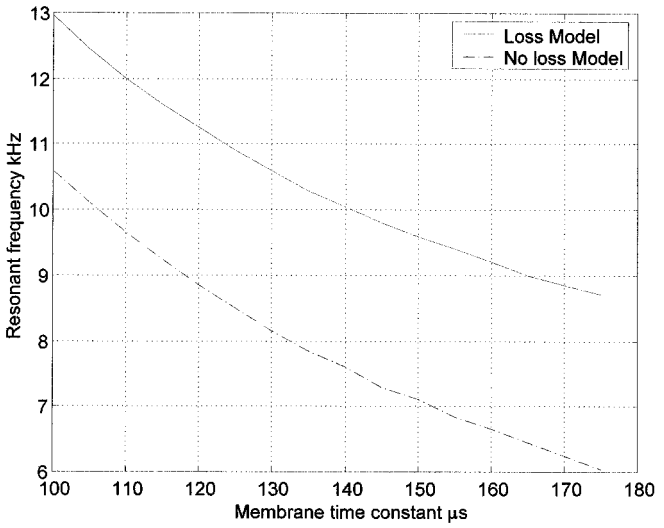

Fig. 6. Optimal resonant frequency as a function of membrane time constant τ_m.

has the lowest negative peak. This is a result of the membrane capacitance.

The problem can be simplified considerably by ignoring resistive loss which hastens the waveform decay. In this limit, the membrane voltage becomes

$$V_m = \delta\omega\sqrt{\frac{2W}{\Re}}\,\frac{\left(\cos(\omega t)+\omega\tau_m\sin(\omega t)-e^{-(t/\tau_m)}\right)}{1+\omega^2\tau_m^2}. \quad (17)$$

The reader is cautioned to exercise care in the use of (17). It is strictly only valid when the resistance is small, i.e., when $\omega\tau_L \gg 1$. All forthcoming plots except Figs. 4 and 7 of this paper are computed using (16).

The equivalent plot to that of Fig. 3 without loss is shown in Fig. 4. Because the resistance is small, little is changed. It is clear that the membrane capacitance contributes to the exponential decay term in (17). This is the reason that the second negative phased pulse is deeper than the positive going wave. As with Fig. 3, an optimal resonant frequency occurs between the extremes of 4 kHz and 20 kHz, with a small monotonic decrease witnessed after 10 kHz. Note that this analysis ignores sodium and potassium gate phenomena which will add additional uncertain time dependent processes.

The numerator is a transcendental equation with no analytical solution for a minimum. The terms $\cos(\omega t)+\omega\tau_m\sin(\omega t)$ have a minimum when

$$\min\{\cos(\omega t)+\omega\tau_m\sin(\omega t)\}\ \text{occurs when}$$
$$t=\frac{\pi+\tan^1(\omega\tau_m)}{\omega}. \quad (18)$$

Equation (16) or (17) can be plotted for a band of resonant frequencies, seeking V_m/δ at the time consistent with (18). Fix the inductance, reluctance, resistance, and capacitance voltage to 21.8 μH, 5.55 10^6 H^{-1}, 12.6 mΩ (6.1 m of #8 copper wire), and 1500 V, respectively. Even with this resistance the absolute value of the second negative, third-quarter minimum is 23% larger than the maximum of the first quarter wave peak. A graph is obtained by allowing the capacitance to span a range

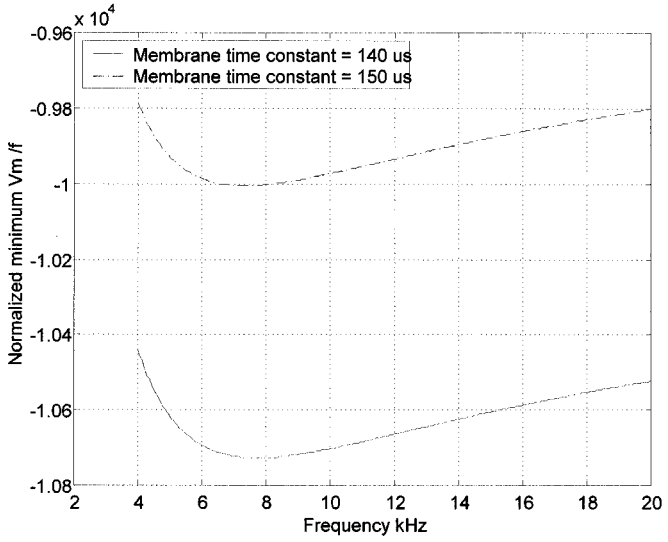

Fig. 7. Membrane voltage V_m as a function of resonant frequency.

of values, but scaling the voltage as the inverse square root of capacitance so the energy remains fixed at 84.4 J. The result for $\tau_m = 125\ \mu$s is a plot closely delivering the optimal circuit resonance frequency shown in Fig. 5. The results are computed with and without losses, and clearly indicate that a lossy system has a higher optimal frequency; the higher frequency allows less time for the exponential L/R decay to dampen the induced membrane voltage. The plots were computed directly over a range of frequencies, and the minimum computed; in addition the minimum was computed directly using (18). The close agreement demonstrates the accuracy of (18) in predicting the peak even in a lossy context. *Remember that the negative peaks are being plotted.* The plot would suggest that a resonant frequency closer to 10 kHz would be ideal for realizing excitation with the smallest energy for this nerve fiber with $\tau_m = 125\ \mu$s. Frequently, component restrictions begin to cause problems before that limit is reached.

Barker [2, Table III] lists a set of mean values for this key time constant τ_m obtained through threshold stimulation on a number of patients. Their results indicated that these time constants ranged from $\tau_m = 121 \pm 23\ \mu$s for peripheral stimulation to $\tau_m = 152 \pm 26\ \mu$s for cortical stimulation. Their ranges considered different degrees of stimulation as well. Shown in Fig. 6 is the optimum circuit resonant frequency as a function of membrane time constant τ_m both with and without losses, with the lossy circuit delivering the higher optimal resonant frequency. The resistance, inductance, and energy parameters are identical to Fig. 5. It is clear from (10) that small nerve fibers have large values of τ_m.

Shown in Fig. 7 is the minimum *negative peak* for V_m as a function of resonant frequency, assuming the resistance of the winding is minimal. The plot is performed under the same conditions as Fig. 3. The larger time constant, 150 μs, corresponds to a smaller fiber. The first important observation is that the negative peak of the larger nerve fiber is greater than for the smaller fiber with the higher time constant τ_m as expected, since smaller fibers are known to be harder to stimulate. The second observation is that the smaller nerve fiber has a smaller optimal resonance frequency.

The results summarized in (16) and (17) lead to several important conclusions. To maximize nerve cell stimulation the following should be observed.

1) Maximize the energy.
2) Minimize the reluctance comprising the magnetic circuit as consistent with the final result in (16). A laminated or tape wound steel core is preferred over air. With magnetic fields characterizing much work in this area where the B field is greater than 1.5 T at the source, a laminated supermendur core which saturates at 2.2 T is preferred over a ferrite core which saturates at 0.45 T, since the latter would have a low reluctance in saturation.
3) Aspire toward a high resonant frequency; depending on the size of the nerve fiber, and target region; this optimal resonant frequency is probably between 9 and 11 kHz in a typical lossy circuit. The resonance frequency can be increased by lowering the turns on the inductor core or by lowering the capacitance, or by lowering both. The inductance of the magnetic circuit becomes dominated by leakage if the turns are too low. If the capacitance is lowered, this recommendation assumes that the operating voltage can be increased to maintain constant energy W.
4) Use a biphasic excitation circuit, since the membrane capacitance will always insure a deeper membrane voltage dip using representative resistances during the second portion of the wave. This result is supported by the recent empirical data of Maccabee [10].

Recommendations 1 and 3 are prone at the writing of this paper to be limited by hardware. The switching apparatus and insulation requirement considerations limit:

a) the maximum operating voltage;
b) the maximum operating current;
c) the maximum resonance frequency that can safely be used to shut off the thyristor before a double firing of that component is witnessed. This number is close to 5 kHz for present state of the art stud mounted SCR devices per manufacturer's recommendations (e.g., Power x). Their turn-off time for a half cycle is about 90 μs.

When the voltage V_C, I, and ω are limited, the components for the stimulator are fixed. As will be shown shortly, the number of turns N does not affect the stimulation voltage, but lowering the exciting circuit resistance will help increase the membrane voltage. This argues for lowering the number of turns. Thus, it forces circuit designer to make the circuit maximum I as large as possible.

IV. Configuration Example

Suppose for the sake of argument that the U.S. Food and Drug Administration (FDA) and component limitations suggest the three following limitations: $V = 2$ kV, $I = 3$ kA, and a complete cycle angular frequency

$$\omega = \frac{2\pi}{200\ \mu\text{s}} = 31\,416. \tag{19}$$

Thyristor shutoff times can be a limiting factor how high the resonant frequency can be raised. If possible the designer should design for the frequency dictated by Fig. 6. (Powerx is stating that new hockey puck SCR's are becoming available with a full cycle time constant of 80–90 μs, shut-off time 40 μs). The reluctance of the core should be as small as possible; some art is involved in the core design since this has to do with tissue depth and target span area. Analytically, the reluctance is the magnetic length divided by the product of the core area, and circuit permeability. This reluctance must be computed numerically using boundary or finite element software for any accuracy. A typical value for a transcranial brain stimulator half toroid spanning 220° made of 3% grain oriented steel is 5.55 10^6 H^{-1}. The two constraints to be enforced relate to energy and resonant frequency

$$\tfrac{1}{2}CV^2 = \tfrac{1}{2}LI^2 \tag{20}$$

$$\omega = \frac{1}{\sqrt{LC}}. \tag{21}$$

Combining these two constraints yields the capacitance C and inductance L as

$$C = \frac{I}{V\omega} = 47.75\ \mu\text{F} \tag{22}$$

$$L = \frac{V}{I\omega} = 21.22\ \mu\text{H}. \tag{23}$$

In terms of the above computed reluctance, the number of turns would be

$$N = \sqrt{L\Re} = \sqrt{(21.22 * 10^{-6})(5.55 * 10^6)} = 10.85\ \text{ turns}. \tag{24}$$

This would be the "ideal" component selection for these conditions. The only way to improve the nerve stimulation further would be to insure that the field from the laminated iron link the target region more effectively, thus, reducing reluctance $\Re$. An adjustment of the turns would be necessary in that event.

The reluctance is obtained using a boundary element or finite element code to find the inductance of a one turn winding carrying the full set of amp-turns under saturation. The design of the core is determined by the width and depth of the target region, and the weight constraint suggested by the physician. For TMS applications, the core is positioned near a motor threshold point manually, and must be manageable by hand. Getting the reluctance in practice is an iterative process. The number of turns is guessed initially. The numerical code returns the reluctance. The turns then follow through (24). The amp-turns are then updated and the process repeated to obtain the reluctance under saturation. These numerical procedures and the core shape are beyond the scope of this paper.

V. Fallacious Conclusions that Result from Ignoring the Membrane Capacitance

A number of erroneous conclusions result from ignoring the membrane capacitance, and focusing only on the exciting circuit. Suppose that all membrane effects are ignored. The induced membrane voltage in the circuit of Fig. 2 will be proportional to the time rate of change of flux $d\Phi/dt$. This quantity can be rearranged in terms of the capacitor voltage V_C as

$$\frac{d\Phi}{dt} = \omega\frac{NI}{\Re} = \frac{NI}{\Re}\frac{1}{\sqrt{LC}} = \frac{N}{\Re}V_C\sqrt{\frac{C}{L}}\frac{1}{\sqrt{LC}} = \frac{N}{\Re}\frac{V_C}{L}. \tag{25}$$

Since inductance is related to N and $\Re$ as

$$L = \frac{N^2}{\Re} \tag{26}$$

the final conclusion would result as

$$\frac{d\Phi}{dt} = \frac{V_C}{N}. \tag{27}$$

Among the erroneous conclusions drawn from (27) would be the following.

1) Changing charging circuit capacitance would have no effect on nerve stimulation.
2) Changing the magnetic reluctance $\Re$ would have no effect on nerve stimulation.
3) Decreasing the number of turns should help stimulate more nerve fibers.

In actuality the following is true:

1) If the energy is held constant, than lowering the capacitance increases the resonant frequency and leads to larger membrane voltage changes.
2) Lowering the magnetic circuit reluctance, lowers the resonant frequency, but increases the achievable membrane voltage change due to the $1/\sqrt{\Re}$ multiplier in (16).
3) Changing the number of turns (e.g., 11 to 9) does not appreciably change the achievable membrane voltage. An advantage is realized to the extent that the total circuit resistance is lowered. In practical circuits, this resistance is typically dominated by parasitic connections and losses in the thyristor.

VI. Conclusion

A coupled magnetic circuit–biological circuit has been formulated in order to predict the conditions for optimizing nerve membrane stimulation. The circuit was formulated using Laplace transform theory. The results of the analysis yield the following four design guidelines.

1) Maximize the energy.
2) Minimize the reluctance.
3) As budget and availability of devices develop, aspire toward a sufficiently high resonant frequency, near 10 kHz.
4) Use a biphasic excitation circuit, since the membrane capacitance will always insure a deeper membrane voltage decrease during the second portion of the wave.

Realistic components and regulations have voltage, current, and switching time limitations. Switching times for stud mounted SCR's are about 200 μs; this is about twice the 100 μs suggested by the theoretical model. The stimulation core must always be designed to deliver the minimum magnetic circuit reluctance under load. This implies a laminated high permeability, low-saturation material having pole spans and head depths sufficient to avoid undue saturation. A detailed analysis of the design of the core head toward this goal requires

a good numerical analysis tool, and is discussed in [11]. Once the maximum operating voltage, current, and minimum switching time are established, the capacitance, inductance, and number of turns for the stimulation core are fixed. Avoid making erroneous design considerations without considering the effect of the nerve membrane capacitance.

For a fixed energy, three changes that help increase membrane voltage are 1) keeping the reluctance low, 2) keeping the resonant frequency up near 7.25–8.75 kHz, and 3) keeping the exciting circuit resistance small. One way to achieve 2) is to lower circuit capacitance C and increase voltage V. Changing the number of turns for a constant energy system has no effect on membrane voltage by itself if the circuit resistance is kept the same; lowering the number of turns is only helpful in that it encourages a lower circuit resistance.

REFERENCES

[1] J. A. Caldwell, "Method and apparatus for magnetically stimulating neurons," U.S. Patent 4 940 453, July 10, 1990.

[2] A. Barker, C. Graham, and I. Freeston, "Magnetic nerve stimulation: The effect of waveform on efficiency, determination of neural time constants, and the measurement of stimulator output," *Magn. Motor Stimulat.: Basic Principles Clin. Experience (EEG Suppl. 43)*, pp. 221–237, 1991.

[3] R. Plonsey, *Bioelectrical Phenomena*. New York: McGraw Hill, 1969, pp. 107–142.

[4] J. A. Cadwell, "Optimizing magnetic stimulator design," *Magn. Motor Stimulat.: Basic Principles Clin. Experience (EEG Suppl. 43)*, pp. 238–248, 1991.

[5] G. A. Mouchawar, J. A. Nyenhuis, J. D. Bourland, and L. A. Geddes, "Guidelines for energy efficient coils: Coils designed for magnetic stimulation of the heart," *Magn. Motor Stimulat.: Basic Principles Clin. Experience (EEG Suppl. 43)*.

[6] C. W. Hess, K. M. Rosler, R. O. Heckmann, and H. P. Ludin, "Magnetic stimulation of the human brain: Influence of size and shape of the stimulating coil," in *Motor Disturbances II*. London, U.K.: Academic, 1990, pp. 31–42.

[7] A. Cantano and P. Noel, "Transcranial magnetic stimulation: Interest in the excitation threshold," *Acta Neurologica Belgica*, vol. 97, p. 61, 1997.

[8] G. Cerri, R. Deleo, F. Moglie, and A. Schiavoni, "An accurate 3-D model for magnetic stimulation of the brain cortex," *J. Med. Eng. Technol.*, vol. 1, pp. 7–16, 1995.

[9] B. J. Roth and P. J. Basser, "A model of the stimulation of a nerve fiber by electromagnetic induction," *IEEE Trans. Biomed. Eng.*, vol. 37, pp. 588–597, June 1990.

[10] P. J. Maccabee, S. S. Nagarajan, V. E. Amassian, D. M. Durand, R. Q. Cracco, A. Z. Szabo, A. Ahad, K. S. Lai, and L. P. Eberle, "Optimal polarity sequence for exciting human and porcine peripheral nerve with neuromagnetic stimuli: With computer simulation," *J. Physiol. (London)*, vol. 513, no. 2, pp. 571–585, 1998.

[11] K. Davey, "Optimizing transcranial magnetic stimulation cores," in *IEEE CEFC 2000 Conf.*, Milwaukee, WI, June 4–7, 2000.

Kent Davey (S'73–M'76–SM'89) received the B.S. degree in electrical engineering from Tulane University, New Orleans, LA, in 1974. From 1974–1976, He completed an M.S. degree in power engineering at Carnegie Mellon University, Pittsburgh, PA, and the M.S. degree in physics at the University of Pittsburgh, Pittsburgh, PA. He completed the Ph.D. degree in electrical engineering at Massachusetts Institute of Technology, Cambridge, in the area of continuum electromechanics in 1979.

From 1974–1976, he worked at Westinghouse Electric, Pittsburgh, PA, in the area of electric machine design. From 1979–1980, he taught as an Assistant Professor at Texas A&M University, Bryan, TX. From 1980–1994, he taught at Georgia Tech, Atlanta, in electrical engineering, reaching the rank of Associate Professor. From 1994–1996, he worked for American Maglev, Inc., Edgewater, FL, as Technical Director for the magnetically levitated train project. From 1996 to the present, he has worked as a Consultant primarily in the area of magnetic nerve stimulation for Neotonus, Inc., a company located in the Atlanta area.

Charles M. Epstein received the A.B. degree in the history of science from Harvard College, Cambridge, MA, in 1969, and the M.D. degree from Harvard Medical School in 1973. During the same time he took courses in biomedical engineering at the Massachusetts Institute of Technology, Cambridge. He trained in Medicine and Neurology at Emory University School of Medicine, Atlanta, GA, from 1973 to 1978, and in Electroencephalography at the Mayo Clinic, Rochester, MN, in 1978.

He is currently Associate Professor of Neurology at Emory University School of Medicine, where he founded the Evoked Potential, Epilepsy, Sleep, and Magnetic Stimulation Laboratories. His major research interests have been quantitative electroencephalography and magnetic stimulation of the nervous system.

In 1999, Dr. Epstein was elected Secretary of the American Clinical Neurophysiology Society.